Anisotropic Electron-Phonon Coupling and Dynamical Nesting on the Graphene Sheets in Superconducting CaC_6 using Angle-Resolved Photoemission Spectroscopy

T. Valla,[1,*] J. Camacho,[1] Z.-H. Pan,[2] A. V. Fedorov,[2] A. C. Walters,[3] C. A. Howard,[3] and M. Ellerby[3]

[1]*Condensed Matter Physics and Materials Science Department, Brookhaven National Laboratory, Upton, New York 11973, USA*

[2]*Advanced Light Source, Lawrence Berkeley National Laboratory, Berkeley, California 94720, USA*

[3]*London Centre for Nanotechnology and Department of Physics and Astronomy, University College London, London WC1E 6BT, United Kingdom*

(Received 7 June 2008; published 13 March 2009)

We present the first angle-resolved photoemission studies of electronic structure in CaC_6, a superconducting graphite intercalation compound with $T_c = 11.6$ K. We find that, contrary to theoretical models, the electron-phonon coupling on the graphene-derived Fermi sheets with high-frequency graphene-derived phonons is surprisingly strong and anisotropic. The shape of the Fermi surface is found to favor a dynamical intervalley nesting via exchange of high-frequency phonons. Our results suggest that graphene sheets play a crucial role in superconductivity in graphite intercalation compounds.

DOI: 10.1103/PhysRevLett.102.107007 PACS numbers: 74.25.Kc, 71.18.+y, 74.10.+v

Superconductivity in graphite intercalation compounds (GIC) has been studied for more than 40 years [1,2] and it is still not fully understood, despite the recent progress and the discovery [3,4] of relatively high T_c superconductivity in CaC_6 and YbC_6. Recent studies now suggest that the electron-phonon coupling (EPC) is most likely responsible for pairing [5–7]. However, it is still not clear whether the graphene-derived electronic states and vibrations, or the intercalant-derived ones play a more important role [8–12]. Most of the theoretical studies suggest that the intercalant-derived Fermi surface (FS) [5] and intercalant-derived soft vibrations [8,9] are the key for superconductivity, while some suggest that the intercalant states couple also to the out-of-plane graphene vibrations [10,11]. However, all of them agree that the graphene electrons are only very weakly coupled to in-plane graphene vibrations, rendering this interaction virtually irrelevant for superconductivity. The most prominent manifestation of EPC is a renormalization of the electronic dispersion or a ''kink'' and the corresponding change in the quasiparticle lifetime at the energy scale associated with the phonons. These effects are directly observable in angle-resolved photoemission spectroscopy (ARPES) [13,14], making this technique an ideal tool for studies of EPC, particularly in anisotropic materials where EPC may display a significant k dependence [15]. Here we present ARPES measurements of the electronic structure in CaC_6 and show that the coupling between graphene-derived π^* electrons and high-frequency graphene-derived phonons is anisotropic and sufficiently strong to induce superconductivity in GICs. Even though we found that the charge transfer from calcium to graphene sheets was not complete, we did not find any evidence of the Ca-derived Fermi surface.

The experiments were carried out on a Scienta SES-100 electron spectrometer operating in the angle-resolved mode at the beam line 12.0.1 of the Advanced Light Source. The spectra presented here were recorded at the photon energy of 45 eV, with the combined instrumental energy resolution of ~20–25 meV and the momentum resolution of ± 0.008 Å^{-1} in geometry where the polarization of light was perpendicular to the probed momentum line. The CaC_6 samples (bulk) were prepared via immersion of a HOPG platelet or natural, single-crystal graphite flake (Madagascan) in a lithium/calcium alloy for 10 days, as described in detail by Pruvost *et al.* [16]. X-ray diffraction showed very high sample purity with no graphite or LiC_6 impurity phases. SQUID magnetometry revealed sharp ($\Delta T < 0.3$ K) superconducting transition at ~11.6 K (onset). To avoid degradation, samples were unsealed and glued to the sample holder with Ag-epoxy in an Ar filled glow box. Protected by the cured epoxy, they were transferred to the ARPES prep-chamber, and cleaved at low temperature (~15–20 K) under ultrahigh vacuum (UHV) conditions (~1×10^{-9} Pa).

The thin flake of pristine graphite was obtained by micromechanical exfoliation of HOPG on a SiO_2/Si substrate in air. From the optical contrast and from Raman data, we determined the thickness of the flake to be in the range of 7–9 graphene layers. The flake was annealed to ~600 K in the UHV chamber before ARPES studies. All the samples were mounted on a high precision variable-temperature goniometer with three angular and three linear degrees of freedom.

Figure 1 shows the ARPES spectra near the K point in the graphene Brillouin zone (BZ) from both CaC_6 and pristine graphite flake. The upper panel (a) shows photoemission intensity from CaC_6 as a function of binding energy for several momentum lines in the vicinity of K point, while the intensity from a narrow interval (± 10 meV) around the Fermi level is shown in the lower panels (b) and (c). For comparison, we also show the ARPES spectrum from the momentum line going through K point (d) and the spectral contours at the Fermi level (e) and at $\omega = -1$ eV (f) of a thin pristine graphite flake (~7–9

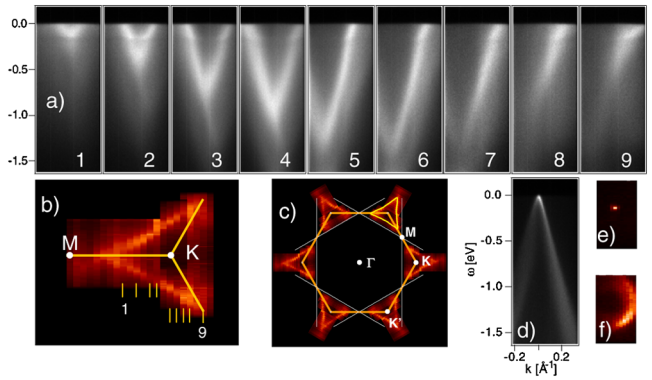

FIG. 1 (color online). (a) 1–9: photoemission spectra from CaC_6 along several momentum lines near the K point as indicated in (b). (b) Photoemission intensity from CaC_6 from a narrow energy interval around the Fermi level ($\omega = \pm 10$ meV) near the K point of the BZ. Thin bars indicate momentum lines probed in (a). (c) Fermi surface of CaC_6 obtained by sixfold symmetrization of intensity shown in (b). White lines correspond to the doping of $1/2$ electrons per C atom, at which the van Hove singularity in the π^* band sits at the Fermi level. (d) ARPES spectrum from a thin pristine graphite flake from the momentum line going through the K point orthogonal to the K-M line. (e) photoemission intensity from the pristine graphite flake around K point at $\omega = 0$ and (f) at $\omega = -1$ eV. All the spectra in (a), (b), (d), (e), and (f) are shown on the same momentum and energy scales and all were taken at $T = 14$ K, in the normal state of CaC_6.

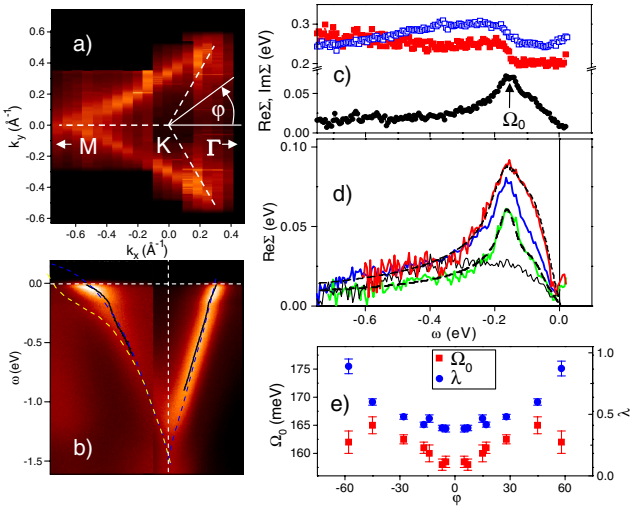

FIG. 2 (color online). (a) Fermi surface of CaC_6. φ defines the polar angle around the K point, measured from the ΓK line. (b) Spectral intensities for $\varphi = 0$ or ΓK line (right) and $\varphi = 180°$ or KM line (left). Black solid lines represent the MDC derived dispersions. Dashed blue (gray) and yellow (light gray) lines represent bands from Ref. [20], calculated for graphene and for CaC_6 monolayer, respectively. (c) ReΣ (black circles) and ImΣ (red solid squares) for $\varphi = 17°$ and ImΣ for $\varphi = 25°$ (blue open squares). Peak (step) position in ReΣ (ImΣ) is labeled with Ω_0. (d) Real part of the self-energy for $\varphi = 7°$, $28°$, and $58°$ (bottom to top). Dashed lines represent the fits to the simple model self-energies as described in text. Thin black line is ReΣ of pristine graphite flake. (e) Characteristic energy Ω_0 of the maximum in ReΣ and the coupling strength λ, extracted from ReΣ as functions of polar angle φ as defined in (a).

graphene layers), on a SiO_2 substrate. A strong anisotropy of photoemission intensity around K point in both systems [panels (b),(c),(f)] is the consequence of electronic chirality and matrix elements [17]. Note that the FS of the pristine graphite collapses nearly into a Dirac point, while the FS of CaC_6 encloses a significant area and has a concave triangular shape centered at the K point of the BZ. The charge transfer from intercalant atoms fills the graphene π^* bands and the Dirac point is moved to $\sim$1.5 eV below the Fermi level. Two important observations about CaC_6 can be made: (1) in all the spectra from Fig. 1(a), there is a renormalization of the quasiparticle dispersion at $\sim$160 meV below the Fermi level and (2) the contour of the spectral intensity at the Fermi level [Figs. 1(b) and 1(c)], corresponding to the graphene-derived FS, is smaller than what would be expected if two Ca electrons were donated to graphene sheets, i.e., if Ca was completely ionized. The area enclosed by these contours corresponds to the doping level of graphene sheets and in the case of complete Ca ionization, this should be $1/6$ of the area of the graphene BZ, equivalent of the doping of $1/3$ electrons per C atom. Instead, the measured Fermi area gives approximately 0.2 electrons per C atom.

It is apparent from Fig. 1 that the renormalization effects (''kinks'') are not equally strong for all the points on the FS of CaC_6 and that they are much stronger than in the pristine graphite. Figure 2 illustrates the anisotropy of the renormalization effects in CaC_6. We have extracted the dispersions and the linewidths of the quasiparticle states by fitting the spectral intensities at constant energies, or momentum distribution curves (MDCs) [13], with Lorentzian distributions. The real and imaginary components of the self-energy are then derived in the usual manner from the peak positions k_m and widths Δk of the MDC peaks at each ω using the expressions

$$\mathrm{Re}\,\Sigma(\omega) = (k_m - k)\nu_0(\omega), \qquad \mathrm{Im}\Sigma(\omega) = \frac{\Delta k}{2}\nu_0(\omega), \quad (1)$$

where $\nu_0(\omega)$ represent the bare band velocity at ω. Here we note that the choice of the bare dispersion may play a significant role in determining the exact shape and magnitude of the self-energy [18]. This has been recently discussed in relation to strong renormalization effects in heavily doped graphene on SiC(0001) [19] and it has been shown that the apparent EPC along the KM lines might be significantly overestimated by the wrong choice of the bare dispersion [20,21]. We have tried to use linear bare dispersions and found that they work reasonably well, except in the very vicinity of the KM lines ($\varphi = \pm 60°$, $180°$), where they may lead to a considerable overestimate of the EPC. We also note that the bands calculated for a CaC_6 monolayer [dashed yellow or light gray line in Fig. 2(b)] [20] do not realistically represent dispersions

measured here. Therefore, we have approximated the bare dispersions with appropriately filled graphene bands from Ref. [20] and found that they work well for the whole FS. The results for $\mathrm{Re}\Sigma$ and $\mathrm{Im}\Sigma$, corresponding to the polar angle $\varphi = 17°$ and $\mathrm{Im}\Sigma$ for $\varphi = 25°$ are shown in Fig. 2(c). Figure 2(d) shows $\mathrm{Re}\Sigma$ for different momentum lines. All the self-energies have a structure typical for the interaction with a well-defined bosonic mode: the imaginary part has a sharp steplike feature, while the real part has a peak at the energy of the mode Ω_0. Therefore, the mode energy can be read from the measured self-energy. In our case, the dominant structure occurs at ~160 meV, with an additional feature at ~75 meV. These features can be naturally attributed to the interaction with in-plane and out-of-plane phonons of the graphene sheets. We note that the finite energy resolution also affects the measured $\mathrm{Re}\Sigma$ near the Fermi level, within the resolution range, but with the tendency to underestimate the measured EPC [22]. We have excluded the affected interval $|\omega| < 20$ meV from the considerations and any fine structure, related to a possible coupling to the intercalant modes, is out of our detection limits. At higher energies, we can model the measured self-energy at any φ with an Eliashberg function $\alpha^2F(\omega)$ consisting of two peaks: one fixed at $\omega = 75$ meV and the other ranging from 155 to 165 meV. The relative contribution of these two peaks increases from 1:5 to almost 1:1 on moving from $\varphi \approx 0$ to $\varphi \approx 60°$. The modeled $\mathrm{Re}\Sigma$ are shown for these two limiting cases. Our model assumes a constant density of states (DOS), whereas a linear DOS would be a better approximation since the scattering is expected to reflect the density of final states. This is visible in Fig. 2(c), where $\mathrm{Im}\Sigma$ quickly acquires a slope as one moves from ΓK to KM. Fitting of measured $\mathrm{Re}\Sigma$ in the energy range $20 \leq |\omega| \leq 300$ meV to the model gives the energy of the high-frequency mode Ω_0. In addition, the coupling strength λ can be extracted from the low energy slope of $\mathrm{Re}\Sigma$, $\lambda = -(\partial \mathrm{Re}\Sigma/\partial\omega)_{\omega\to 0}$. From Fig. 2(d) it is clear that the characteristic energy Ω_0 does not vary a lot, whereas the coupling strength λ displays a significant anisotropy. In Fig. 2(e), we plot both quantities as functions of polar angle φ. The coupling constant ranges from 0.38 (for $\varphi \approx 0$) to 0.89 (for $\varphi \approx 60°$), with the momentum averaged value of 0.53. The coupling constant in pristine graphite flake is much smaller ($\lambda = 0.16$) and does not show a significant anisotropy, in agreement with Leem *et al.* [23]. Recent theoretical calculations suggest that in CaC_6, the crucial role is played by calcium, i.e., electrons on the intercalant-derived FS couple strongly to the intercalant vibrations [8–11]. Those calculations show nearly 1 order of magnitude weaker coupling of the graphene-derived electrons to the in-plane graphene phonons, with essentially no anisotropy [24]. The large calcium isotope effect also implies the dominant role of soft Ca vibrations in superconductivity [7]. Our results, on the contrary, suggest that graphene sheets play the dominant role because the obtained EPC on graphene-derived FS with the in-plane and out-of-plane graphene phonons seems to be more than sufficient to give $T_c \approx 11.6$ K.

Where is such strong and anisotropic coupling coming from? Similar anisotropy was recently reported for EPC in K and Ca doped graphene on SiC [19]. There, the proximity of van Hove singularity (vHS) to the Fermi level was suggested to be an origin of the enhanced EPC. Even though the claim on very high anisotropy was subsequently retracted due to the erroneous procedure of extracting EPC near the KM lines, the measured coupling on the unaffected portion of the FS was still significantly stronger than the calculated one [21]. In the case of CaC_6 we believe that we have found the mechanism of enhancement of EPC: very favorable dynamical nesting conditions exist on the FS that may strongly enhance the *intervalley* EPC. In an intervalley scattering, an electron is scattered from one

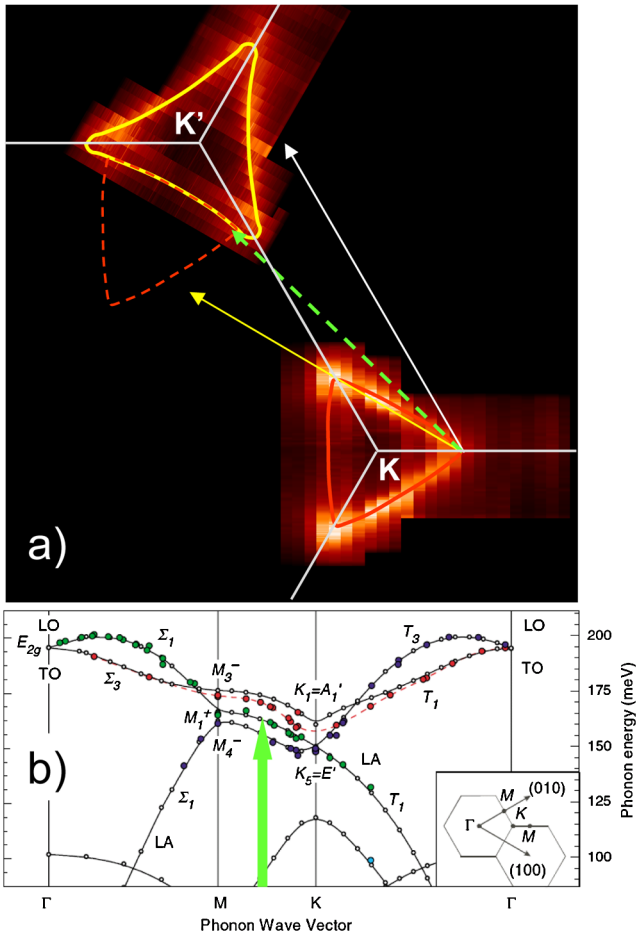

FIG. 3 (color online). (a) Contour of photoemission intensity from CaC_6 at $\omega = 0$ (Fermi surface) around K' point (yellow or light gray contour) and at the "kink" energy, $\omega = -160$ meV, (red or gray contour) in the vicinity of K point of the BZ. White (yellow or light gray) arrow represents the ΓK (ΓM) wave vector, while the dashed green arrow represents the wave vector that efficiently "nests" the two contours. (b) Phonon dispersions in pristine graphite from Ref. [25]. The position of dynamical "nesting" wave vector from (a) is marked with green arrow whose length corresponds to the exchanged energy.

valley to another ($K \rightarrow K'$ or $K' \rightarrow K$). This is illustrated in Fig. 3. In order to satisfy the energy conservation rule in an electron-phonon scattering event, the photohole created at ~160 meV has to be scattered to the Fermi level after emission of a 160 meV phonon. To explore the allowed momenta in such a process, we plot the states at $\omega = -160$ meV at one corner of the BZ (K) and the states at the Fermi level in another corner (K'). A wave vector connecting any pair of points on different contours represents an allowed scattering process. Note that in the case of *intravalley* scattering, both contours would have to be centered at the same K or K' point. However, from the measured phonon spectra in graphite [25], and recent Raman experiments on CaC_6 [26], it is clear that there are no $q \sim 0$ modes at ~160 meV and we have to consider intervalley scattering. From Fig. 3(a), it appears that some wave vectors are particularly efficient in connecting the two contours. As the $\omega = -160$ meV contour is slightly convex and the FS is slightly concave with nearly the same curvature, the dashed green vector in Fig. 3(a) effectively nests the whole side, or ~1/3 of the length of the two contours. We note that the observed "nesting" is not static: it involves emission/absorption of a high-frequency phonon and would not produce the charge density wave (CDW) instability. The dynamical nesting and resulting enhancement of EPC is likely to be very sensitive to the filling of graphene-derived bands. For lower doping levels, the nesting efficiency might be quickly lost as both contours become convex. At even higher fillings, possibly realized under pressure, the nesting conditions would likely improve further, but at some point, the coupling to lower frequency phonons near the KM lines might become too strong and eventually drive the system into the CDW state.

The measured Fermi velocity on the graphene-derived FS is also very anisotropic: $\nu_F(\varphi = 180°) \approx 1.1$ eV Å, $\nu_F(\varphi = 0) \approx 4.1$ eV Å, with the momentum average $\langle \nu_F \rangle \approx 2.5$ eV Å. If the graphene electrons were responsible for superconducting properties, $\langle \nu_F \rangle$ would correspond to the in-plane coherence length, $\xi_{ab} = \hbar \nu_F / (\pi \Delta)$ of approximately 500 Å if we take $\Delta \approx 1.6$ meV for the superconducting gap [27], in reasonable agreement with $\xi_{ab} \approx 350$ Å reported in STM [27], specific heat [5], and magnetization [4,6] studies. We also note that peculiar linearity in the upper critical filed, H_{c2}, at low temperatures, could also be explained by anisotropic Fermi velocity on the graphene-derived FS [8]. In contrast, the intercalant bands are predicted to be free-electron–like, with a 3-dimensional, nearly spherical FS and would not produce linear H_{c2}. We have searched for these bands at several photon energies, ranging from 40 to 75 eV, and found no evidence of the intercalant-derived FS. However, our results show that, irrespectively of whether the intercalant band is occupied or not, the measured EPC on the graphene-derived FS to the high-frequency graphene phonons alone might be more than sufficient to explain relatively high T_c in CaC_6. Thus, in addition to the amazing properties in the charge-neutral state [28], graphene sheets also show surprises in the heavily doped regime: they may support strong pairing interactions and lead to superconductivity in compounds in which they are building blocks.

We acknowledge technical help from Antony Bollinger and useful discussions with Phil Allen, Matteo Calandra, Peter Johnson, Myron Strongin, Alexei Tsvelik, and Mary Upton. The research work described in this Letter was supported by the U.S. Department of Energy and the U.K. Engineering and Physical Science Research Council.

*valla@bnl.gov

[1] N. B. Hannay *et al.*, Phys. Rev. Lett. **14**, 225 (1965).
[2] M. S. Dresselhaus and G. Dresselhaus, Adv. Phys. **51**, 1 (2002).
[3] T. E. Weller, M. Ellerby, S. S. Saxena, R. P. Smith, and N. T. Skipper, Nature Phys. **1**, 39 (2005).
[4] N. Emery *et al.*, Phys. Rev. Lett. **95**, 087003 (2005).
[5] J. S. Kim, R. K. Kremer, L. Boeri, and F. S. Razavi, Phys. Rev. Lett. **96**, 217002 (2006).
[6] G. Lamura *et al.*, Phys. Rev. Lett. **96**, 107008 (2006).
[7] D. G. Hinks, D. Rosenmann, H. Claus, M. S. Bailey, and J. D. Jorgensen, Phys. Rev. B **75**, 014509 (2007).
[8] G. Csányi, P. B. Littlewood, A. H. Nevidomskyy, C. J. Pickard, and B. D. Simons, Nature Phys. **1**, 42 (2005).
[9] I. I. Mazin, Phys. Rev. Lett. **95**, 227001 (2005).
[10] M. Calandra and F. Mauri, Phys. Rev. Lett. **95**, 237002 (2005).
[11] L. Boeri, G. B. Bachelet, M. Giantomassi, and O. K. Andersen, Phys. Rev. B **76**, 064510 (2007).
[12] I. I. Mazin *et al.*, Physica (Amsterdam) **460C**, 116 (2007).
[13] T. Valla, A. V. Fedorov, P. D. Johnson, and S. L. Hulbert, Phys. Rev. Lett. **83**, 2085 (1999).
[14] M. Hengsberger, D. Purdie, P. Segovia, M. Garnier, and Y. Baer, Phys. Rev. Lett. **83**, 592 (1999).
[15] T. Valla *et al.*, Phys. Rev. Lett. **92**, 086401 (2004).
[16] S. Pruvost, C. Hérold, A. Hérold, and P. Lagrange, Carbon **42**, 1825 (2004).
[17] Kruczynski *et al.*, Phys. Rev. B **77**, 195403 (2008).
[18] T. Valla *et al.*, Phys. Rev. Lett. **85**, 4759 (2000).
[19] J. L. McChesney *et al.*, arXiv:0705.3264.
[20] M. Calandra and F. Mauri, Phys. Rev. B **76**, 161406(R) (2007).
[21] C.-H. Park *et al.*, Phys. Rev. B **77**, 113410 (2008).
[22] T. Valla, Phys. Rev. Lett. **96**, 119701 (2006).
[23] C. S. Leem *et al.*, Phys. Rev. Lett. **100**, 016802 (2008).
[24] C.-H. Park, F. Giustino, M. L. Cohen, and S. G. Louie, Phys. Rev. Lett. **99**, 086804 (2007).
[25] J. Maultzsch, S. Reich, C. Thomsen, H. Requardt, and P. Ordejón, Phys. Rev. Lett. **92**, 075501 (2004).
[26] J. Hlinka *et al.*, Phys. Rev. B **76**, 144512 (2007).
[27] N. Bergeal *et al.*, Phys. Rev. Lett. **97**, 077003 (2006).
[28] A. K. Geim and K. S. Novoselov, Nature Mater. **6**, 183 (2007).